European Polymer Journal 241 (2025) 114389

Contents lists available at ScienceDirect

European Polymer Journal

journal homepage: www.elsevier.com/locate/europolj

Tunable phenolic-modified alginate–chitosan semi-IPNs as multifunctional platforms for localized antimicrobial and antioxidant therapy

Elisabetta Grazia Tomarchio [a,b], Chiara Zagni [a,*], Giusy Curcuruto [c], Virginia Fuochi [b], Salvatore Furnari [b], Pio Maria Furneri [b], Sabrina Carola Carroccio [c], Antonio Rescifina [a]

[a] Department of Drug and Health Sciences, University of Catania, V.le A. Doria 6, 95125 Catania, Italy
[b] Department of Biomedical and Biotechnological Sciences, University of Catania, Via Santa Sofia 97, 95123 Catania, Italy
[c] Institute for Polymers, Composites, and Biomaterials CNR-IPCB, Via Paolo Gaifami 18, 95126 Catania, Italy

ARTICLE INFO

Keywords:
Hydrogel
semi-IPN
Lomefloxacin
Alginate
Chitosan
Drug delivery

ABSTRACT

Biopolymer-based hydrogels offer a versatile platform for drug delivery thanks to their biocompatibility, use of natural polymers, and tunable properties. In this study, we developed semi-interpenetrating polymer network (semi-IPN) hydrogels composed of alginate (ALG) and chitosan (CS), chemically modified with caffeic acid (CA) and gallic acid (GA), to enhance both antimicrobial and antioxidant activity. The resulting hydrogels showed tunable physical states, high porosity, and good thermal stability, transitioning from liquid dispersions to solid forms under different conditions. Lomefloxacin was loaded to test local delivery performance. Drug release profiles revealed that the modification influenced release: the ALG-CS_CA hydrogel released about 61 % of Lomefloxacin, while the ALG-CS_GA hydrogel released approximately 43 %, in line with their swelling behavior. Incorporation of phenolic acids significantly boosted antioxidant capacity, with the GA-modified hydrogel reaching over 80 % scavenging activity. Tests against *Staphylococcus aureus* confirmed improved antimicrobial activity compared to unmodified ALG-CS matrices. Overall, these fully bio-based, metal-free semi-IPNs combine biocompatibility, antimicrobial and antioxidant functions, and tunable release properties. This sustainable system, based only on natural polymers and mild chemical functionalization, shows strong potential for safe, scalable biomedical applications in localized therapies for infection-prone or inflamed tissues. This green design offers practical advantages for future scale-up and sustainable production.

1. Introduction

Natural polymers have gained significant attention in the development of drug delivery systems due to their remarkable advantages, including excellent biocompatibility, biodegradability, and low cytotoxicity. Among these, hydrogels have emerged as an up-and-coming class of materials, owing to their ability to retain large amounts of water while maintaining a flexible structure [1,2]. This unique characteristic enables them to provide controlled and sustained release of therapeutic agents, making them ideal candidates for various biomedical applications, such as wound healing, tissue engineering, and drug delivery [3,4]. Hydrogels, due to their water-swelling properties, can also offer advantages in drug encapsulation and local delivery, ensuring prolonged and efficient therapeutic effects [5].

Among the natural polymers, alginate, an anionic polysaccharide extracted from brown algae, is known for its excellent gel-forming ability in the presence of divalent cations (e.g., Ca^{2+}) [6]. This property, coupled with its high biocompatibility, mucoadhesive nature, and its ability to form stable gels under physiological conditions, makes alginate particularly suitable for encapsulating and delivering a variety of therapeutic agents, including proteins, peptides, and small molecules [7]. Moreover, alginate's ability to undergo controlled degradation further enhances its potential in drug delivery applications, allowing for the design of systems that release drugs over an extended period. For example, floating mucoadhesive alginate beads loaded with clarithromycin have been developed to target Helicobacter pylori infections in the gastric mucosa [8].

On the other hand, chitosan (CS), a natural polysaccharide derived from chitin, has gained significant interest due to its broad-spectrum antibacterial properties, biodegradability, and excellent biocompatibility [9]. These properties make it an ideal candidate for drug-delivery applications, particularly in mucoadhesive formulations, which can

* Corresponding author.
E-mail address: chiara.zagni@unict.it (C. Zagni).

https://doi.org/10.1016/j.eurpolymj.2025.114389
Received 11 September 2025; Received in revised form 28 October 2025; Accepted 3 November 2025
Available online 5 November 2025

provide enhanced residence time at the site of administration [10]. Furthermore, CS can be readily functionalized to improve its physicochemical properties, such as hydrophilicity, mechanical strength, and bioactivity, thereby making it even more versatile for biomedical applications [11].

The combination of alginate and chitosan into semi-interpenetrating polymer networks (semi-IPNs) leverages the mechanical robustness of ionically crosslinked alginate with the tunability and bioactivity of chitosan, yielding hydrogels with enhanced stability, swelling behavior, and rapid release, while retaining a fraction of the drug within the hydrogel network [7,12,13]. The electrostatic interaction between the anionic carboxyl groups of alginate and the cationic amino groups of chitosan significantly improves gel stability, swelling, and drug release under physiological conditions, allowing efficient delivery of therapeutic agents while enhancing their stability, bioavailability, and bioactivity [14,15].

For instance, IPN hydrogels of sodium alginate and chitosan were developed for the delivery of deferoxamine, a highly water-soluble iron-chelating agent [16]. These systems, processed as spray-dried hydrogel microspheres, effectively encapsulated deferoxamine and allowed for modulation of its release, highlighting the potential of alginate–chitosan matrices for managing hydrophilic drugs. These systems, based on alginate–chitosan matrices, have also been used for enzyme delivery. In this context, Wu *et al.* developed innovative hydrogels composed of chitosan and sodium alginate (CS-ALG) for the encapsulation and protection of lysozyme. The resulting system exhibited high enzyme loading efficiency, significant swelling capacity, and enhanced antibacterial activity [17]. Due to their high biocompatibility, these systems have also been utilized as scaffolds in tissue engineering applications, exhibiting excellent cell adhesion properties and facilitating effective tissue regeneration [18].

Recent studies have explored phenolic acid-functionalized chitosan integrated into alginate-based semi-IPNs, including cryogels and microgels, imparting antioxidant and antimicrobial properties, modulating network morphology, and enabling tailored drug delivery. Caffeic acid (CA) primarily enhances antimicrobial activity, whereas gallic acid (GA) contributes to antioxidant performance [19]. These natural polyphenols introduce additional hydroxyl and aromatic groups that facilitate interactions with both organic and inorganic substrates via hydrogen bonding or hydrophobic interactions, thereby conferring enhanced antioxidant and antimicrobial activities, as well as improved solubility and physicochemical stability [3,20].

Several studies report that chitosan-CA conjugates achieve significantly enhanced antioxidant and antimicrobial performance compared to the native polymer, up to 5-fold higher radical scavenging and substantial activity against methicillin-resistant *S. aureus* [21], whereas chitosan-GA conjugates show potent ABTS and DPPH quenching even at low concentrations [22]. In our system, the alginate–chitosan network provides the structural scaffold, while phenolic acid grafting is the key factor responsible for the improved functional properties. The contribution of CA or GA grafting should therefore be regarded as the dominant mechanism driving bioactivity, with the polymer matrix ensuring stability and integrity of the semi-IPN. GA predominantly enhances antioxidant performance, whereas CA mainly contributes to antimicrobial functionality. Thus, the modification does not merely add bioactive functions but produces a material in which the structural scaffold and phenolic grafting together determine its overall functional performance. The incorporation of chemically modified chitosan within the IPN's network boosts bioactivity, imparting antioxidant and antimicrobial functionalities essential for localized therapeutic applications [7]. Despite these advances, studies integrating phenolic-modified chitosan within alginate–chitosan semi-IPNs remain scarce, and the distinct contribution of each phenolic modification to overall performance remains underexplored.

Our study builds on these advancements by investigating caffeic and gallic acid modifications on the physicochemical properties, swelling, and drug release kinetics of alginate-chitosan semi-IPNs, providing new insights into structure–function relationships for biomedical applications.

In this study, we designed phenolic acid-modified semi-IPN hydrogels by combining alginate with chitosan chemically grafted with caffeic and gallic acids. This approach aims to address the main drawbacks of pure alginate hydrogels by leveraging the stabilizing and bioactive contributions of modified chitosan, while enhancing its intrinsic antibacterial and antioxidant properties. As a proof-of-concept, the fluoroquinolone antibiotic lomefloxacin (Lome) was incorporated into these hydrogel systems to target resistant *Staphylococcus aureus* infections, a common cause of opportunistic infections [23]. Localized therapy is particularly critical for *S. aureus* infections because this pathogen has a strong biofilm-forming capacity, rendering systemic antibiotic therapy ineffective. Within biofilms, *S. aureus* cells are embedded in a protective extracellular matrix that reduces antibiotic penetration and shields them from host immune defenses, leading to chronic, relapsing infections [24]. Moreover, *S. aureus*, including MRSA strains, shows high rates of antibiotic resistance, and local delivery offers the dual advantage of (i) achieving high concentrations of antimicrobials at the infection site while (ii) minimizing systemic side effects and the risk of resistance development [25]. The physical tunability of these hydrogels enables them to transition from injectable liquids to temperature-responsive gels and, upon freeze-drying, to porous solids, allowing multiple routes of administration, such as spray delivery, and thereby enhancing their versatility for biomedical applications. These features are particularly advantageous for localized drug delivery, as they support rapid release and subsequent retention of a fraction of the drug within the hydrogel network, thereby improving drug bioavailability and residence time at the infection site. For localized infections, this rapid initial release is particularly desirable, as it allows therapeutic drug concentrations to be reached quickly at the site of infection [26].

2. Experimental

2.1. Materials

Sodium alginate (product code A2033), derived from brown algae and purchased from Sigma-Aldrich, has medium viscosity, a molecular weight of 80,000–120,000 Da, and a mannuronic (M) to guluronic (G) residue ratio M/G = 1.56. Chitosan (product code C2395), obtained from TCI, has an average molecular weight of approximately 200 kDa and a viscosity of 5–20 mPa·s, measured at 0.5 % (w/v) in 0.5 % acetic acid at 20 °C. The degree of deacetylation is approximately 80 %, as determined by ^{1}H NMR. Caffeic acid (CA), gallic acid (GA), *N*-(3-dimetilaminopropil)-*N*′-etilcarbodiimide (EDC), *N*-Hydroxysuccinimide (NHS), acetic acid, calcium chloride ($CaCl_2$), acetone, and ethanol were purchased from Merck. A Milli-Q water purification system was used to produce deionized water. ^{1}H NMR spectrum was recorded at 300 K on Varian UNITY Inova 400 MHz using deuterium oxide (D_2O) and aceticacid-d_4 (CD_3COOD).

The bacterial strain *Staphylococcus aureus* (ATCC 25213) was sourced from the American Type Culture Collection (ATCC, Manassas, VA, USA).

2.2. Chemistry

2.2.1. Synthesis of chitosan-gallic acid (CS_GA)

The preparation of CS_GA involved a carbodiimide-mediated coupling strategy with slight modifications [27]. Briefly, 0.5 g of chitosan (CS) was solubilized in 10 mL of 2 % (v/v) acetic acid. In parallel, 561.4 mg (3.3 mmol) of gallic acid (GA) was dissolved in ethanol under magnetic stirring. 1.89 g (9.9 mmol) of 1-ethyl-3-(3-dimethylaminopropyl)carbodiimide (EDC) and 1.14 g (9.9 mmol) of *N*-hydroxysuccinimide (NHS) were dissolved in 10 mL of water at controlled acidity (pH 5.5) and added to the GA solution. The resulting mixture was kept at 0 °C for 1 h to initiate the activation process. The CS solution was

slowly introduced to the activated GA solution, and the reaction was maintained at the same temperature for an additional 30 min. The system was then stirred at room temperature for 12 h to allow complete conjugation. Then, cold acetone was added, and the precipitate was collected and washed several times with ethanol to remove excess reactants. The modified chitosan was then dried at room temperature, diluted in water, and freeze-dried to yield a whitish solid. ^{1}H NMR (400 MHz, D_2O) δ 7.09 (s, 2H, GA) 3.83–3.68 (m, H3, H4, H5, H6 CS), 3.10 (s, H2 CS), 1.99 (s, 3H, CH_3, *N*-acetyl CS).

2.2.2. Synthesis of chitosan-caffeic acid (CS_CA)

The synthesis of CS_CA was performed using the same procedure as for caffeic acid, including purification. Specifically, 0.5 g of CS, 594.5 mg of caffeic acid (CA), 1.89 g (9.9 mmol) of 1-ethyl-3-(3-dimethylaminopropyl)carbodiimide (EDC), and 1.14 g (9.9 mmol) of *N*-hydroxysuccinimide (NHS) were used. ^{1}H NMR (400 MHz, D_2O) δ 7.50 (d, J = 15.9 Hz, 1H, CA) 7.12 (d, 1H, CA), 7.05 (dd, J = 8.3, 21 Hz, 1H, CA), 6.87 (d, J = 8.2 Hz, 1H, CA), 6.28 (d, J = 15.9 Hz, 1H, CA), 3.83–3.69(m, H3, H4, H5, H6 CS), 3.09 (s, H2 CS), 1.98 (s, 3H, CH_3 *N*-acetyl CS).

2.2.3. General procedure for the synthesis of semi-IPN hydrogel

Preparation of the Alginate Solution: 1 % w/v sodium alginate solution was prepared by dissolving 20 mg of sodium alginate in 2 mL of deionized water. The mixture was magnetically stirred at 40 °C until complete dissolution and allowed to rest for 30 min to eliminate air bubbles.

Preparation of the Chitosan Solution: a 1.5 % w/v chitosan solution was prepared by dissolving 30 mg of CS in 2 mL of 2 % (v/v) acidic water and magnetically stirring at 40 °C until complete dissolution.

Preparation of the Crosslinking Solution: a 0.5 % w/v calcium chloride ($CaCl_2$) solution was prepared by dissolving 10 mg of $CaCl_2$ in 2 mL of deionized water.

Formation of the Semi-IPN Gels: The alginate solution was gradually added dropwise to the CS solution under constant stirring (300 rpm) at room temperature to ensure homogeneous mixing of the polymers. Subsequently, 2 mL of the 0.5 % w/v $CaCl_2$ solution was slowly added to the polymeric mixture under continuous stirring at 4 °C to achieve controlled, uniform crosslinking of sodium alginate [28]. The system was stirred for 30 min to complete the crosslinking process.

The polymer gel obtained exhibited a high degree of physical tunability under different post-processing conditions. At room temperature, the formulation appeared as a viscous gel suitable for handling and further processing. Upon freeze-drying, the gel was converted into solid, porous scaffolds that conformed to the container's geometry. To obtain solid disk samples with homogeneous weight and structure, approximately 1 mL of the polymeric mixture was cast into cylindrical molds corresponding to the wells of a 24-well plate, yielding samples with an average dry weight of ~ 50 mg per sample. All dried samples exhibited a uniform shape and size, ensuring reproducibility across different batches and suitability for subsequent physicochemical characterization, drug release studies, and antimicrobial assays. Conversely, freezing followed by gel thawing produced compact hydrogels that retained the mold-defined geometry.

Different samples were prepared using either pristine or functionalized chitosan (CS). The obtained samples were named *ALG-CS*, *ALG-CS_CA*, and *ALG-CS_GA*.

Formation of the Semi-IPN/Lome Gels: The semi-IPN gels containing Lome were prepared following the same procedure. Lome (20 mg) was added during the polymer dissolution process. The resulting samples were named *ALG-CS_CA/Lome and ALG-CS_GA/Lome*.

2.3. Characterization

2.3.1. Infrared spectroscopy (FT-IR)

FTIR-ATR analysis was carried out using an Agilent Cary 630 FTIR spectrometer with an ATR sampling module. The spectra were collected over 64 scans in the 4000–500 cm^{-1} range, with a resolution of 4 cm^{-1}, at room temperature.

2.3.2. Thermogravimetric analysis (TGA)

TGA was performed with a TA Instruments Q500 system under a nitrogen atmosphere (flow rate of 60 mL/min). The analysis was conducted at a heating rate of 10 °C/min over a temperature range of 40–800 °C. The instrument provides a sensitivity of 0.1 μg, a weighing precision of ± 0.01 %, and an isothermal temperature accuracy of ± 1 °C.

2.3.3. Scanning electron microscopy (SEM)

Morphological characterization of semi-IPNs was performed using a Thermo Phenom ProX desktop SEM (Thermo Fisher Scientific, Waltham, MA, USA). Samples were mounted on an aluminum stub with double-sided adhesive tape and analyzed without a conductive coating, using an appropriate sample holder. To further quantify pore features, the SEM micrographs were processed using Phenom Porometric software v.1.1.2.0 (Phenom-World BV, Eindhoven, The Netherlands).

2.4. Swelling test

The semi-IPN swelling properties were evaluated by measuring its solvent absorption capacity. Initially, the IPN samples were dried in an oven at 50 °C until they reached a constant weight. The dry weight (W_0) was recorded using an analytical balance with a precision of 0.01 mg. Afterward, the dried samples were soaked in both distilled water and phosphate-buffered saline (PBS) at room temperature for 1 h. Once the swelling process was complete, the samples were taken out, carefully blotted with filter paper to remove excess water, and weighed (W_s) [29].

The swelling ratio (SR) was calculated using Equation (1):

$$SR = \frac{(W_s - W_0)}{W_0} \quad (1)$$

All experiments were performed in triplicate, and the results are presented as mean values with standard deviation.

2.5. In vitro drug release

The *in vitro* release studies of Lome were conducted to evaluate the concentration of the released compound over time in PBS (pH 7.4) and acetate buffer (pH = 5.0). All release experiments were performed under constant agitation using an orbital shaker at moderate velocity at room temperature. An appropriate amount of polymer (10 mg) was dispersed in an equal amount of release media (10 mL). At predetermined time intervals (0, 5, 10, 20, 30, 45, 60, 100, 120, 180 min, and 24 h), aliquots (200 μL) of the sample solution were withdrawn and immediately replaced with an equal volume of fresh solution to maintain a constant volume. The absorbance of the solution was measured using a UV–Vis spectrophotometer at the appropriate wavelength (281 nm in PBS buffer). The concentration of the released compound was determined using a calibration curve of Lome in PBS. All drug release experiments were performed in triplicate. Data are expressed as mean values ± standard deviation.

2.6. Kinetics of release

The release profile of Lome from ALG-CS-based semi-IPN hydrogels was evaluated by fitting the experimental data to various mathematical models commonly applied in drug delivery studies, including zero-order, first-order, Higuchi, Korsmeyer–Peppas, and Weibull models [30]. Data analysis was performed using GraphPad Prism 9, and the quality of fit for each model was assessed using the coefficient of determination (R^2). The model showing the highest R^2 was considered the most representative of the release mechanism.

2.7. Antioxidant assay

The antioxidant activity of the composite semi-IPN hydrogels was evaluated using a modified version of the previously described method [27]. To assess the DPPH free radical scavenging activity, 2.5 mg of CS, ALG-CS_CA, and ALG-CS_GA were immersed in 2 mL of a 0.02 mM DPPH anhydrous ethanol solution. The mixture was vortexed and incubated in the dark for 30 min. The absorbance of the resulting solution was then measured at 517 nm. The DPPH scavenging activity percentage (SA) of the semi-IPN hydrogels was calculated using the formula in Equation (2):

$$SA = \frac{(A_0 - A_1)}{A_0} \times 100 \quad (2)$$

where A_0 is the absorbance of the control (DPPH solution without sample) and A_1 is the absorbance of the sample with DPPH.

2.8. Antimicrobial activity

The antibacterial activity of the semi-IPNs against *Staphylococcus aureus* ATCC 25213 was evaluated using the agar disk diffusion method. Bacterial strain was sourced from the American Type Culture Collection (ATCC, Manassas, VA, USA). Before testing, the hydrogel disks were sterilized by UV irradiation for 30 min. Solid semi-IPN disks were placed on Muller-Hinton (MH) agar (Thermo Scientific™ Oxoid™) plates pre-inoculated with the pathogen. A disk of Lome 10 μg (Thermo Scientific™ Oxoid™ CT1661B) was used as an internal control. Plates were incubated aerobically at 37 °C overnight, and the inhibition zones were measured in mm utilizing a caliper [31].

The antibacterial activity of semi-IPNs was also quantitatively assessed under dynamic contact conditions in accordance with ASTM E2149. In brief, sterile semi-IPNs were individually placed into 250 mL sterile flasks containing 50 ± 0.5 mL of a working bacterial suspension of *Staphylococcus aureus* ATCC 25213. The bacterial inoculum was prepared from an overnight culture grown in Tryptic Soy Broth (TSB) at 35 ± 2 °C and diluted in sterile phosphate-buffered saline (PBS) to a final concentration of 1.5–3.0 × 10^5 CFU/mL. Then, flasks were incubated at 37 °C for 18 h under constant agitation using a wrist-action shaker to ensure uniform contact between the hydrogels and bacterial cells. After incubation, serial ten-fold dilutions were prepared in PBS, and 100 μL aliquots of appropriate dilutions were plated in triplicate on Plate Count Agar (PCA). Following overnight incubation at 37 °C, colonies were enumerated, and results were expressed as % of reduction using Equation 3:

$$\%\,Reduction = \frac{B - A}{B}\, x\, 100 \quad (3)$$

where A is the treated samples and B is the inoculum-only control.

All assays were performed in triplicate, and values were reported as mean ± standard deviation.

3. Results and discussion

3.1. Synthesis of functionalized polymeric materials

Chitosan-based formulations have been extensively studied for their antibacterial, antiviral, and antioxidant properties, to enhance their solubility and bioactivity. In this work, chitosan was chemically modified via targeted grafting reactions at its amino groups using carboxyl-containing compounds. The functionalization was carried out following widely established catechol grafting methods [27]. Caffeic acid and gallic acid were conjugated to chitosan via EDC/NHS-mediated carboxyl coupling, enhancing their mucoadhesive properties [32–34].

The success of the grafting reactions was confirmed by ^{1}H NMR spectroscopy, which revealed characteristic peaks corresponding to the newly introduced functional groups. In particular, the functionalization of chitosan with caffeic acid was evidenced by the appearance of signals in the aromatic region (6.2–7.5 ppm), attributed to the protons of the catechol ring, along with peaks corresponding to the olefinic protons of the conjugated double bond (Fig. 1b). Similarly, gallic acid grafting was confirmed by the presence of the aromatic protons signals at 7.09 ppm [22]. These spectral features, along with thermogravimetric analysis data (Fig. S1), provided clear evidence of successful grafting and the structural modifications of chitosan.

To develop mucoadhesive hydrogels for localized drug delivery, a semi-interpenetrating polymer network (semi-IPN) was designed using sodium alginate and either pristine or functionalized chitosan. The choice of these polymers was driven by their well-established biocompatibility, biodegradability, and film-forming properties, which are essential for mucosal applications.

Hydrogels were formulated by mixing sodium alginate with either pristine or functionalized chitosan, followed by the addition of $CaCl_2$ crosslinking agent to induce gelation (Fig. 2). This process stabilized the structure through ionic interactions, leading to the formation of a cohesive network. To systematically assess the impact of functionalization, three distinct formulations were prepared: the reference system (ALG-CS) using unmodified chitosan, and two modified systems (ALG-CS_CA and ALG-CS_GA) incorporating chitosan grafted with caffeic or gallic acid, respectively. This comparative approach enabled evaluation of how phenolic grafting influences the hydrogel's structural integrity and bioactive potential. For drug incorporation, lomefloxacin was added directly during polymer dissolution, ensuring homogeneous distribution within the gel matrix. The resulting drug-loaded hydrogels (ALG-CS_CA/Lome and ALG-CS_GA/Lome) were designed to maximize drug retention and enhance localized antimicrobial efficacy.

Interestingly, the resulting materials showed a high degree of physical tunability under different post-processing conditions. In their native state, all formulations exhibited a liquid-like behavior, enabling facile administration, including via sprayable routes such as nasal delivery (Figs. 2a and b). Upon storage at sub-zero temperatures (−20 °C), the materials underwent physical gelation, forming stable, soft hydrogels. The mechanism of cryogel formation involves freezing most of the solvent into ice crystals, while a fraction remains unfrozen. The solutes are expelled from the ice and concentrated in the unfrozen microdomains, where polymerization and/or interpolymer interactions proceed. The ice crystals act as porogens, resulting in an interconnected macroporous structure upon thawing [35]. This reversible phase change highlights their potential for temperature-triggered applications. Furthermore, upon freeze-drying, the hydrogels were converted into solid, porous scaffolds with preserved structural integrity. This dry, porous architecture is particularly advantageous for applications involving storage stability and controlled drug delivery. The high porosity also provides greater surface area, enhancing drug loading efficiency and facilitating faster rehydration at the target site. In addition, Fig. 2d illustrates the specific chemical interactions established between the semi-IPN matrix and Lome, including hydrogen bonding and other non-covalent forces. These interactions are crucial for stabilizing the drug within the polymeric network, thereby influencing both loading efficiency and release behavior. The versatility in physical states (liquid, gel, and solid) opens up avenues for customizable administration strategies, positioning these semi-IPN materials as promising candidates for advanced, adaptable biomedical applications.

3.2. Characterization of semi-IPN

Interpreting the FTIR spectra is challenging due to overlapping absorption bands arising from the various components within the system. Fig. 3a shows the spectra of chitosan (CS), alginate (ALG), and their complex (ALG-CS). The broad O–H/N–H band at 3300–3400 cm^{-1} is present in all samples, while shifts in this region in the ALG-CS spectrum

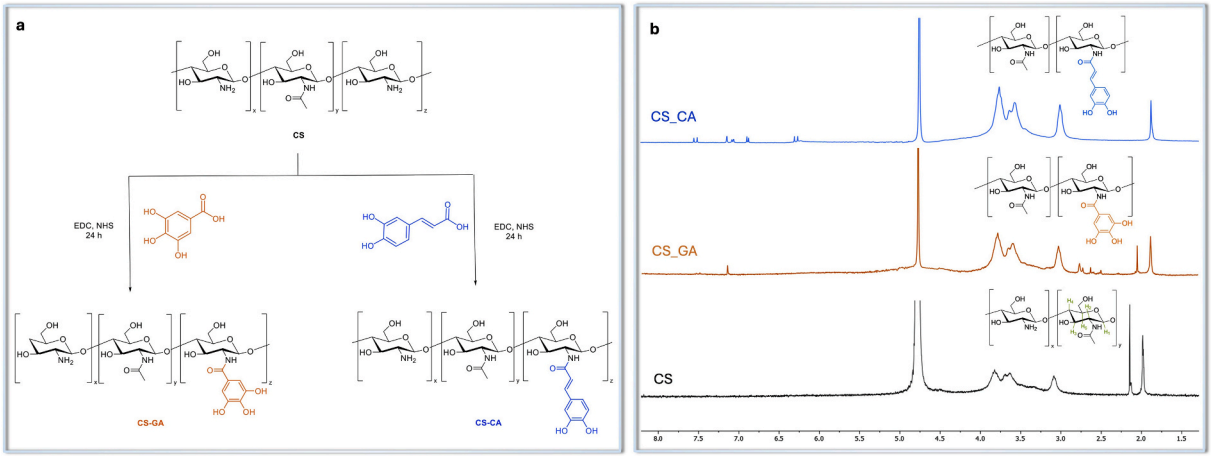

Fig. 1. (a) Synthetic procedure for the synthesis of CS_GA and CS_CA; (b) ^{1}H NMR spectra of CS, CS_GA, and CS_CA.

indicate hydrogen bonding or electrostatic interactions. Moreover, changes in the COO^{-} stretching region (1600–1400 cm^{-1}) and in the carbohydrate backbone signals (1200–1000 cm^{-1}) confirm the formation of a polyelectrolyte complex between ALG and CS, rather than a simple physical mixture. The FTIR spectra of the chitosan, caffeic acid, and ALG-CS_CA are also reported in Fig. 3b. In the spectrum of CS, a broad absorption band centered at 3420 cm^{-1} is ascribed to O–H and N–H stretching vibrations. Additional bands located at 1638, 1423, and 1322 cm^{-1} are attributed to the C=O stretching of the N-acetyl group (amide I), N–H bending of primary amines (amide II), and C–N stretching within the N-acetyl group (amide III), respectively. The FTIR spectrum of the ALG-CS_CA composite exhibits characteristic amide bands at 1640 cm^{-1} (amide I), 1550 cm^{-1} (amide II), and 1300 cm^{-1} (amide III), in agreement with previous findings on chitosan-based systems [36]. A comparative analysis of the spectra reveals increased intensity of the amide bands in ALG-CS_CA relative to pure chitosan, which may reflect the amide bond formation between chitosan and caffeic acid. Furthermore, the observed shift of the amide I and II bands toward lower wavenumbers suggests the successful incorporation of caffeic acid moieties into the chitosan backbone and supports the formation of covalent amide linkages.

Fig. 3c displays the FTIR spectra of gallic acid (GA) and the ALG-CS_GA hybrid. In the GA spectrum, the absorption bands at 3495 and 3284 cm^{-1} correspond to O–H stretching vibrations associated with the aromatic ring, while the peak at 1541 cm^{-1} is assigned to the C=C stretching vibration within the aromatic system. Following conjugation with chitosan, the spectrum of ALG-CS_GA retains the broad absorption at 3420 cm^{-1}, consistent with the presence of O–H and N–H stretching modes. The persistence of the 1541 cm^{-1} band confirms the successful introduction of GA into the polymeric network. This spectral evolution suggests that the primary amine groups of chitosan have undergone nucleophilic substitution with the carboxyl groups of GA, forming secondary amide bonds.

The SEM analysis of the freeze-dried hydrogels highlights how chitosan modification influences the internal architecture of the semi-IPN matrices. In Fig. 3d, the unmodified ALG-CS hydrogel shows a compact, disordered structure with poorly defined pores and limited interconnectivity. Figs. 3e–f, related to gallic acid- and caffeic acid-functionalized chitosan, respectively, reveal highly porous, fibrous networks with interconnected, wrinkled walls. This morphology indicates strong interpolymer interactions, likely due to hydrogen bonding and electrostatic attraction, which supports the formation of a well-integrated semi-IPN.

Automated analysis confirmed significant porosity in the phenolic-functionalized semi-IPNs and revealed notable differences between the two modified hydrogels (Fig. S2). The ALG-CS_GA hydrogel (Fig. 3e) showed slightly smaller pores, ranging from 10 to 110 μm. These pore size distributions are also summarized in Fig. S2. In comparison, the ALG-CS_CA hydrogel (Fig. 3f) exhibited a highly porous structure with larger pore sizes, ranging from 15 to 120 μm.

The data on degradation temperatures (T deg) shown in Table 1 reveal interesting differences among the samples we analyzed. ALG-CS shows a relatively high degradation temperature of 267 °C [37]. In comparison, the functionalized hydrogels, ALG-CS_CA and ALG-CS_GA, exhibit degradation temperatures of 266 °C and 281 °C, respectively. ALG-CS exhibited a residual mass of 14 %, which is typical for hydrogels with moderate crosslinking. In contrast, the functionalized hydrogels, ALG-CS_CA and ALG-CS_GA, exhibited higher residual masses (28 % and 30 %, respectively), confirming increased carbonaceous char formation due to the aromatic polyphenol content and functionalization of the network.

Two key factors explain the enhanced thermal stability observed for the gallic acid-modified hydrogel (ALG-CS_GA) [38]. First, gallic acid exhibits higher antioxidant activity than caffeic acid, thereby improving the thermal stability of the hydrogel by protecting the polymer chains from oxidative degradation during heating, especially under an inert (nitrogen) atmosphere. Second, gallic acid has a 3,4,5-trihydroxybenzoic structure, providing three aromatic hydroxyl (–OH) groups, while caffeic acid has only two such hydroxyls. The greater number of phenolic groups in GA favors stronger hydrogen bonding and more extensive intermolecular interactions within the polymer network, mechanistically enhancing network cohesion, increasing crosslinking density, and allowing higher char residue formation upon heating. This effect is clearly reflected in the higher degradation temperature (281 °C) and the higher residue (30 %) observed for ALG-CS_GA compared to the caffeic acid counterpart (266 °C, 28 %). Thus, the stability gain with GA derives from both superior antioxidant properties and more effective stabilization of the semi-IPN structure via denser hydrogen bonding and π-π interactions.

3.3. *Swelling test*

The swelling behavior of the synthesized semi-IPNs highlights the crucial impact of chitosan functionalization on water uptake, primarily through modifications of the material's ionic properties and network structure. The swelling response is significantly influenced not only by the intrinsic characteristics of the base polymers but also by the chemical modifications introduced [17]. The semi-IPN composed of pristine alginate and chitosan (ALG-CS) exhibited the highest swelling ratio in water (49), rapidly forming a stable hydrogel-like structure (Fig. 4). This pronounced swelling can be attributed to the abundance of free amino groups in CS and carboxyl groups in ALG, which promote extensive ionic

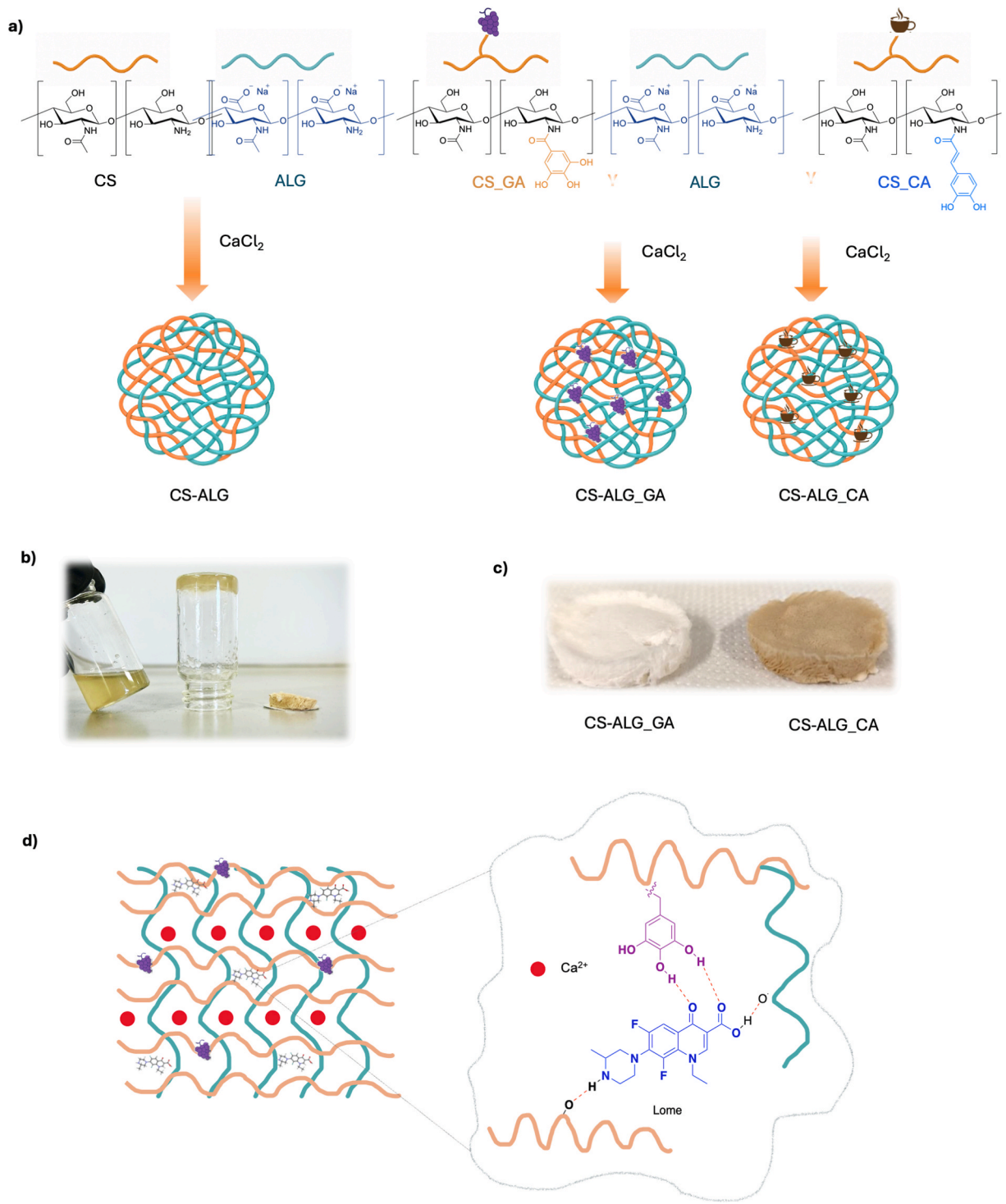

Fig. 2. (a) Schematic representation of semi-IPN preparations; (b) physical forms of CA-ALG semi-IPN; (c) freeze-fried functionalized CS_ALG; d) chemical interactions between semi-IPN and Lome.

interactions with water molecules, resulting in high water retention. Conversely, the semi-IPN containing modified CS exhibited markedly lower water swelling ratios (9), likely due to a combination of reduced ionic character and increased steric hindrance resulting from chemical functionalization. The introduction of bulky substituents onto the CS backbone not only limits the availability of ionic sites capable of interacting with water but also physically restricts the expansion of the polymer network, thereby impairing its swelling capability. Interestingly, in PBS, the swelling behavior followed a different trend. The semi-IPN composed of pristine CS showed a lower swelling ratio (18), whereas the semi-IPN containing chitosan modified with caffeic acid (ALG-CS_CA) exhibited a significantly higher swelling capacity (36.8). This enhancement can be explained by multiple cooperating factors that combine ion-exchange and ionic interaction. Firstly, the significant contribution arises from ion-exchange processes between Na^{+} ions in PBS and Ca^{2+} ions at the alginate crosslinking sites. Specifically, substituting the crosslinking Ca^{2+} with a monovalent Na^{+} ion weakens the ionic junctions that stabilize the alginate network, thereby reducing

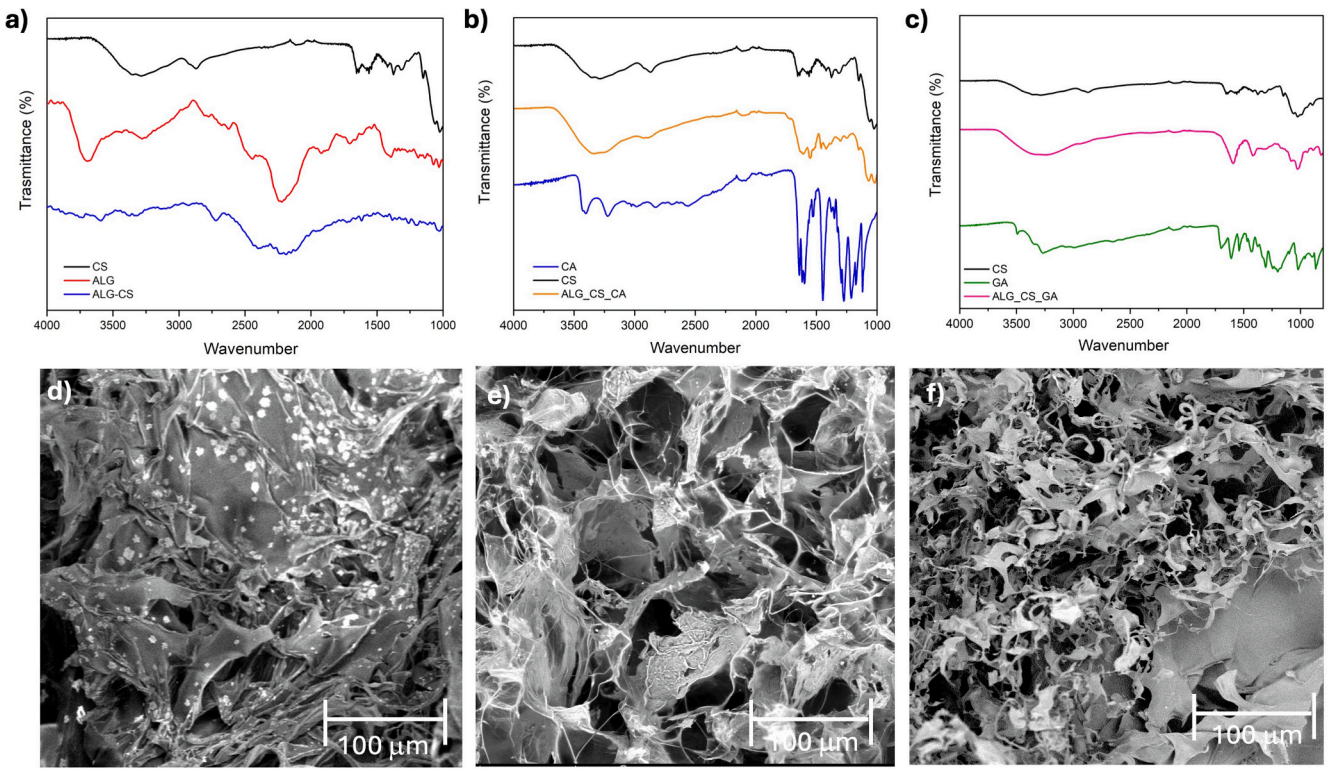

Fig. 3. IR spectra of CA, ALG, and ALG-CS (a), CA, CS, and ALG-CS_CA (b), and CS, GA, and ALG-CS_CA (c). SEM images of ALG-CS (d), ALG-CS_GA (e), and ALG-CS_CA (f).

Table 1
Degradation temperature and mass loss percentages of the synthesized hydrogels.

Sample	T deg (°C)	Residue %
ALG-CS	267	14
ALG-CS_CA	266	28
ALG-CS_GA	281	30

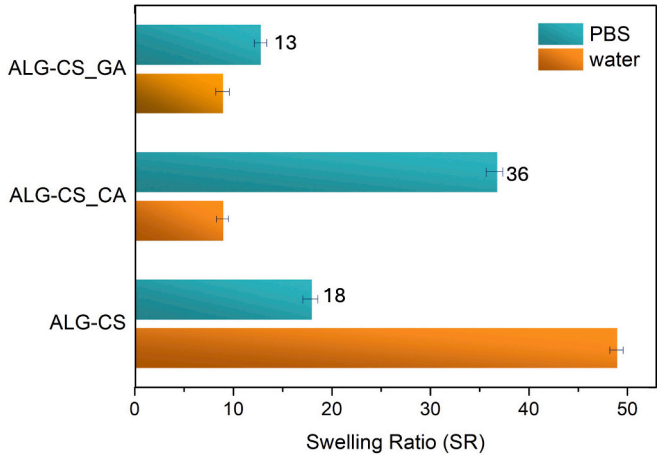

Fig. 4. Swelling ratio of semi-IPNs.

crosslink density and enhancing water uptake [39]. Secondly, the caffeic acid grafting further amplifies this effect: bulky aromatic substituents disrupt polymer packing, increasing free volume and improving ion accessibility and mobility within the matrix. Additionally, phosphate anions in PBS can interact with protonated amino groups on chitosan, contributing to osmotic imbalance and secondary swelling. In general, high ionic strength environments tend to suppress hydrogel swelling via Donnan osmotic effects, in which mobile counterions reduce the internal osmotic pressure, leading to shrinkage. However, in our case, the prevailing ion-exchange ($Na^{+} \leftrightarrow Ca^{2+}$) and ionic interaction mechanisms overcome this tendency, leading to a reversal of the swelling trend compared to pure water [40]. In contrast, the semi-IPN based on chitosan functionalized with gallic acid (ALG-CS_GA) displayed only a modest swelling in PBS (12.8), indicating that the nature of the chemical modification critically influences the hydrogel's swelling response under different ionic environments.

3.4. Drug release

The drug release behavior of the semi-IPNs was investigated to evaluate their potential as hydrogels for rapid, localized drug delivery. Functionalized chitosan derivatives (ALG-CS_CA and ALG-CS_GA) were synthesized and crosslinked with sodium alginate in the presence of $CaCl_2$ to form hydrogel networks entrapping Lomefloxacin (Lome) during the gelation process [41].

The release study was conducted in phosphate-buffered saline (PBS, pH 7.4) at 37 °C to simulate physiological ionic strength and temperature, mimicking in vivo conditions for localized mucosal applications. Absorbance measurements were used to determine Lome concentrations based on a pre-established calibration curve [42]. The semi-IPN structure controls drug release *via*: (i) ionic interactions between ALG and Ca^{2+}, which influenced the porosity and swelling behavior of the network, and (ii) the chemical modification of chitosan with phenolic acids, which modulated drug-polymer interactions [43,44]. The presence of CA and GA moieties significantly affected both the hydrophilicity and electrostatic interactions within the hydrogel, leading to distinct drug release profiles [22].

Drug release showed marked differences among the samples, reflecting variations in matrix swelling and drug-polymer interactions.

The modification of chitosan with catechol altered the release kinetics [45]: in PBS, ALG-CS_CA released approximately 61 % of the drug, while ALG-CS_GA reached only ~ 43 % and displayed a plateau after 60 min (Fig. 5a). These results are consistent with the swelling behavior of the hydrogels, which showed that ALG-CS_CA had a higher swelling ratio in PBS (36.8) compared to ALG-CS_GA (12.8), despite both having identical swelling in water. This suggests that the gallic acid-functionalized matrix expands less in ionic environments, likely due to increased crosslinking or to oxidative changes in GA during gelation that reduce its hydrophilicity and water interactions [46]. In particular, the reduced release of ALG-CS_GA can be rationalized by the specific chemical features of gallic acid. Its aromatic ring provides hydrophobic domains within the otherwise hydrophilic hydrogel, enabling π-π stacking with the quinolone ring of Lome, while its three hydroxyl groups form multiple hydrogen bonds with the drug's carboxyl and amino groups [47]. These interactions stabilize drug–polymer complexes and limit drug mobility. Moreover, GA incorporation contributes to a denser network structure, as evidenced by higher TGA residue (~30 %), supporting enhanced crosslinking and char formation. Together, these effects (stronger matrix binding and increased crosslinking) contribute to reduced swelling and to the observed early plateau in release [48].

The overall drug release profile of ALG-CS_GA suggests stronger drug–matrix interaction or reduced matrix relaxation, which impairs diffusion, despite the presence of hydrophilic groups. In contrast, ALG-CS_CA exhibits more efficient water uptake and drug diffusion in PBS, resulting in faster release. Lome release was also monitored up to 24 h to better characterize the release profile over an extended period. While a significant fraction of the drug (~60 % for ALG-CS_CA, ~43 % for ALG-CS_GA) was released rapidly within the first 30–60 min, the subsequent plateau indicates that the remaining drug is retained mainly within the hydrogel matrix, with minimal further diffusion under the conditions tested, rather than following classical long-term sustained release. This rapid release followed by retention is suitable for localized infection therapy, where achieving high local concentrations quickly is critical. Complete drug release from these semi-IPN hydrogels would likely require hydrogel network degradation, which is not achieved under the current experimental conditions.

The acidic pH release study was performed to simulate wound or infection environments, where local acidification is often present. The cumulative release of Lome observed for all formulations was markedly higher at acidic pH than in PBS. Specifically, the maximum release after 240 min increased to ~ 69 % for ALG_CS, ~87 % for ALG_CS_CA, and ~ 59 % for ALG_CS_GA in acetate buffer (Fig. S3). This enhanced release at lower pH is attributed to the increased protonation of chitosan amino groups, which promotes electrostatic repulsion between the hydrogel matrix and the drug, as well as higher solubility of the encapsulated molecule, both factors known to facilitate drug diffusion and release from the network. These results are consistent with previously reported pH-responsive chitosan-based hydrogels, where acidic conditions accelerate and amplify drug release via matrix swelling and reduced drug–matrix affinity [47].

To better understand the release mechanisms, the experimental data were fitted to various kinetic models, including zero-order, first-order, Higuchi, Korsmeyer–Peppas, and Weibull models. Fig. 5b illustrates, as a representative example, the fitting of the ALG-CS data, while the fittings for ALG-CS_CA and ALG-CS_GA are provided in Fig. S4, along with a table containing the corresponding data and equations (Table S1).

For ALG-CS_CA, the Weibull model provided the best fit (R^2 = 0.9802), with a shape parameter $b = 0.1213$, indicating a release profile characterized by a decreasing release rate over time. This behavior is consistent with a diffusion-controlled mechanism (Fickian or quasi-Fickian), where an initial burst is followed by sustained slower release, in agreement with the swelling and polymer–drug interaction data.

For ALG-CS_GA, the Korsmeyer–Peppas model provided a better fit ($R^2 = 0.8917$) with a release exponent $n = 0.2081$, indicating a Fickian diffusion-controlled release mechanism. This low n value suggests that drug release is primarily governed by diffusion through the hydrogel matrix, consistent with the observed premature plateau in the release profile and stronger drug–matrix interactions limiting matrix relaxation.

These results highlight the significance of selecting appropriate kinetic models to elucidate the underlying release mechanisms and guide the design of tailored drug delivery systems. Overall, the semi-IPNs demonstrate rapid release followed by retention within the hydrogel network influenced by chemical functionalization, ionic crosslinking, and network swelling, offering a versatile platform for localized antibiotic delivery under physiological conditions.

3.5. Antioxidant activity

The antioxidant capacity of the semi-IPN hydrogels was evaluated by measuring their DPPH radical scavenging activity [49]. The unmodified chitosan hydrogel exhibited the lowest scavenging activity, with a value of 20.30 ± 1.06 %, likely due to the limited availability of free amino groups to interact with DPPH radicals (Fig. 6). In contrast, hydrogels containing phenolic acid-functionalized chitosan showed significantly enhanced antioxidant activity. Specifically, the ALG–CS–GA hydrogel demonstrated a marked increase in radical scavenging activity, exceeding 80 %, attributable to the incorporation of gallic acid, a polyphenolic compound known for its strong hydrogen-donating capacity. Similarly, the ALG-CS_CA hydrogel exhibited antioxidant activity reaching approximately 60 %, highlighting the beneficial effect of caffeic acid grafting. As a positive control, ascorbic acid was employed, exhibiting a scavenging activity above 90 % under the experimental conditions. The comparison clearly demonstrates that both phenolic-modified hydrogels exhibit superior antioxidant performance relative

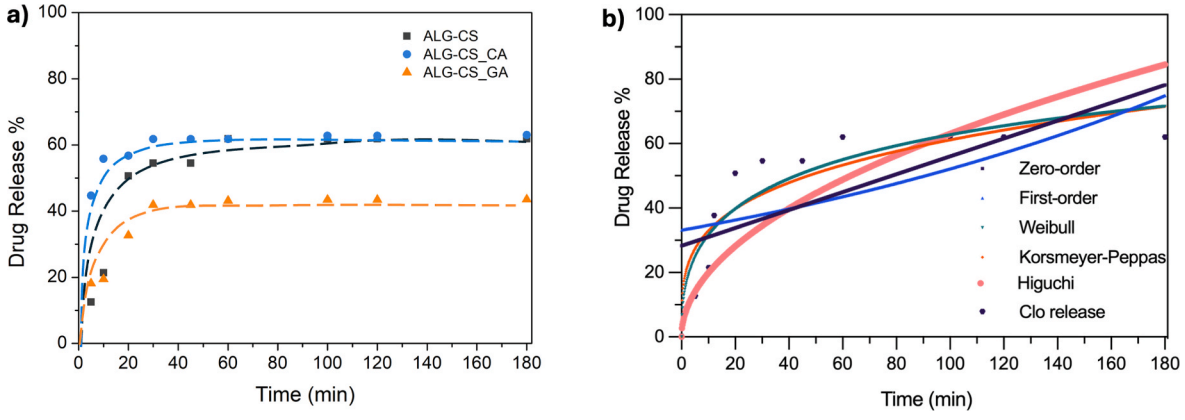

Fig. 5. (a) Lome release percentage from synthesized semi-IPNs in PBS; (b) Fitting curve of Lome release from the ALG_CS system.

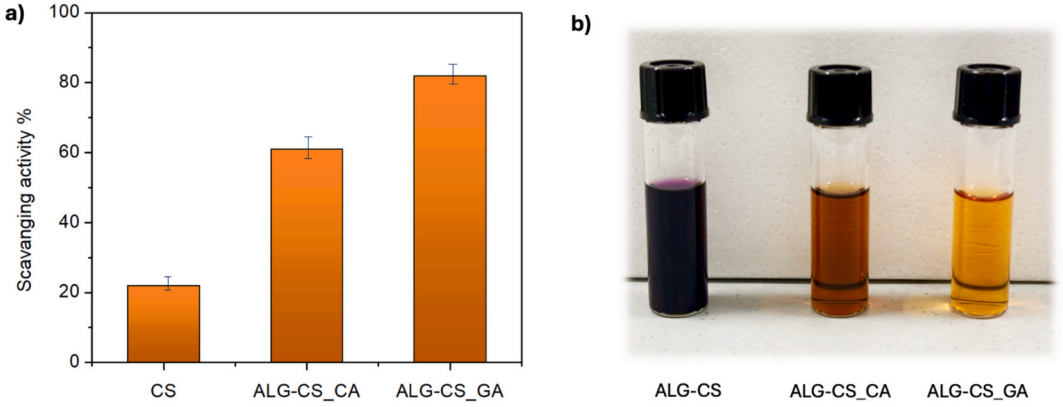

Fig. 6. (a) Scavenging activity (%) and (b) representative of DPPH assay of semi-IPN systems.

to unmodified chitosan. The antioxidant activity is primarily due to the phenolic –OH groups of the grafted polyphenols, which donate electrons or hydrogen atoms to neutralize free radicals such as DPPH and Reactive oxygen species (ROS) [50]. This enhanced antioxidant activity is important not only for improving the stability and shelf-life of the hydrogels but also for their antimicrobial performance. ROS contribute to bacterial defense mechanisms, and the presence of antioxidants can disrupt these systems, rendering bacteria more vulnerable to antimicrobial agents [51]. Therefore, the combined antioxidant and antimicrobial properties of these hydrogels may synergistically enhance their therapeutic efficacy.

3.6. Microbiological tests

Semi-IPNs, including those loaded with caffeic acid, gallic acid, and their respective combinations, were tested against *S. aureus* to evaluate their antibacterial activity. As shown in Table 2, significant antibacterial activity was primarily exhibited by hydrogels loaded with Lome (Fig. 7), with inhibition zones of 38.80 ± 0.2 mm in ALG-CS_CA/Lome, 38.10 ± 0.3 mm in ALG-CS_GA/Lome, and 39.50 ± 0.3 mm in ALG-CS/Lome. These values were significantly higher than those for free Lome alone (22.60 ± 0.1 mm), suggesting a potentiation effect provided by the hydrogel matrix.

Among the antibiotic-free hydrogels, ALG-CS_CA was the only formulation to display notable antibacterial activity, with an inhibition zone of 25.15 ± 0.2 mm, supporting the intrinsic antimicrobial potential of caffeic acid when incorporated into the polymeric network. Conversely, both ALG-CS and ALG-CS_GA showed no detectable antibacterial effect (inhibition zone ≤ 6 mm), consistent with the absence of active antimicrobial agents or possible inactivation of gallic acid during processing. In particular, the lack of activity for ALG-CS_GA can be ascribed to the covalent immobilization of gallic acid within the chitosan network, which severely restricts its accessibility and thus bioactivity. This interpretation is strongly supported by recent literature, which shows that gallic acid exhibits markedly reduced antimicrobial activity when immobilized or loaded into polymeric matrices compared to its free form [26]. Supporting data indicate that freely dissolved gallic acid consistently generates larger inhibition zones and lower bacterial counts than its polymer-bound counterparts.

Table 2
Summary of the results from both the agar diffusion assay (results are indicated as the mean of the measurement ± 0.1 mm) and the broth assay (results are shown as the percentage of inhibition).

Sample	Inhibition zone (mm)	Inhibition %
ALG-CS	≤6	NR
ALG-CS/Lome	39.50 ± 0.3	100
ALG-CS_CA	25.15 ± 0.2	58
ALG-CS_CA/Lome	38.80 ± 0.2	100
ALG-CS_GA	≤6	NR
ALG-CS_GA/Lome	38.10 ± 0.3	100
Lome	22.60 ± 0.1	100

*≤6 no inhibition zone; NR no reduction.

Results obtained from the dynamic flask assay were consistent with those from the disk diffusion method. Results showed that ALG-CS hydrogels loaded with Lome achieved a 100 % reduction in viable *S. aureus* cells after 18 h of incubation. This complete inhibition of bacterial growth is likely attributable to the high concentration of Lomefloxacin released during the contact period.

Among the antibiotic-free hydrogels, the ALG-CS_CA formulation exhibited a 58 % reduction in bacterial counts, confirming the inhibitory effect previously observed in the disk diffusion assay. The consistency between the two assay types supports the dual functionality of the designed system, suggesting that incorporating bioactive polyphenols can significantly enhance both antioxidant and antimicrobial properties.

In contrast, the ALG-CS_GA hydrogel did not exhibit measurable antibacterial activity under dynamic conditions, consistent with the lack of inhibition observed in the agar diffusion assay. This discrepancy, despite the well-documented antimicrobial potential of gallic acid, may be explained by its rapid oxidative degradation during gelation or storage, leading to a loss of bioactivity.

4. Conclusions

In this work, we successfully developed and thoroughly characterized a novel class of semi-interpenetrating polymer network hydrogels based on alginate and chitosan, chemically functionalized with phenolic compounds (caffeic acid and gallic acid) to enhance the system's bioactivity. These multifunctional hydrogels were explicitly designed to address localized infections and oxidative stress, combining antimicrobial and antioxidant properties within a single platform.

The integration of natural polyphenols not only improved the antioxidant potential of the hydrogels, as evidenced by the DPPH radical scavenging assay, but also contributed to their intrinsic antimicrobial efficacy, especially in the caffeic acid-modified formulation. Loading with the antibiotic lomefloxacin enabled sustained, controlled drug release, thereby supporting prolonged therapeutic action. Notably, the hydrogels exhibited tunable physical states, transitioning reversibly from liquid dispersions to solid porous scaffolds, a feature that enhances their versatility for different administration routes and localized delivery.

The ALG-CS semi-IPN hydrogels also displayed favourable physicochemical characteristics, including pronounced porosity, thermal stability, and responsiveness to environmental stimuli, which together contribute to their versatility as drug delivery systems. Notably, the use of only naturally derived polymers and mild, metal-free

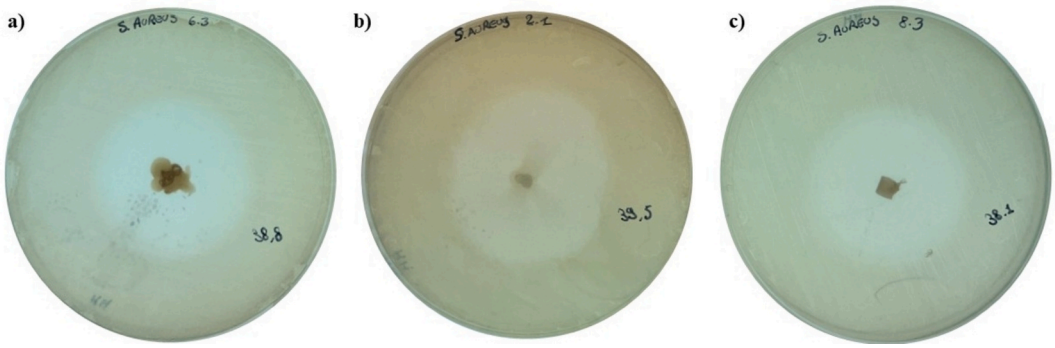

Fig. 7. Representative images of a single replicate showing the antibacterial activity against *S. aureus* of different hydrogel formulations incorporating Lome. (a) ALG-CS_CA/Lome, (b) ALG-CS/Lome, (c) ALG-CS_GA/Lome.

functionalization steps ensures high biocompatibility and environmental sustainability. This green and easily scalable strategy makes these systems promising candidates for industrial production and real-world biomedical applications. To our knowledge, this is the first demonstration of phenolic-modified alginate–chitosan semi-IPNs combining tunable physical states, dual antimicrobial and antioxidant activity, and sustained drug release in a single, green platform. Future work will further investigate their *in vivo* performance and potential for clinical translation.

CRediT authorship contribution statement

Elisabetta Grazia Tomarchio: Writing – original draft, Methodology, Investigation, Conceptualization. **Chiara Zagni:** Writing – review & editing, Writing – original draft, Validation, Investigation, Formal analysis, Data curation, Conceptualization. **Giusy Curcuruto:** Writing – original draft, Validation, Investigation. **Virginia Fuochi:** Writing – original draft, Validation, Methodology. **Salvatore Furnari:** Methodology, Investigation. **Pio Maria Furneri:** Writing – review & editing, Resources. **Sabrina Carola Carroccio:** Writing – review & editing, Supervision, Resources, Project administration. **Antonio Rescifina:** Writing – review & editing, Resources, Project administration, Funding acquisition.

Funding

This research was partially funded by the European Union (Next-Generation EU) through the MIUR-PNRR project SAMOTHRACE-Sicilian MicronanoTech Research and Innovation Center (ECS00000022, CUP B63C22000620005).

Declaration of competing interest

The authors declare that they have no known competing financial interests or personal relationships that could have appeared to influence the work reported in this paper.

Appendix A. Supplementary data

Supplementary data to this article can be found online at https://doi.org/10.1016/j.eurpolymj.2025.114389.

Data availability

No data was used for the research described in the article.

References

[1] A. Mahmood, D. Patel, B. Hickson, J. DesRochers, X. Hu, Recent progress in biopolymer-based hydrogel materials for biomedical applications, Int. J. Mol. Sci. 23 (2022) 1415, https://doi.org/10.3390/ijms23031415.
[2] M. Gosecka, M. Gosecki, D. Jaworska-Krych, Hydrophobized hydrogels: construction strategies, properties, and biomedical applications, Adv. Funct. Mater. 33 (2023) 2212302, https://doi.org/10.1002/adfm.202212302.
[3] N. Bhattarai, J. Gunn, M. Zhang, Chitosan-based hydrogels for controlled, localized drug delivery, Adv. Drug Deliv. Rev. 62 (2010) 83–99, https://doi.org/10.1016/j.addr.2009.07.019.
[4] Y.-Q. Liu, H. Li, Z.-W. Wang, C.-Y. Hu, X. Xu, Superstretchable and tough physical cross-linking hydrogels with dual pH and temperature responsiveness for in vivo treatment of *Staphylococcus aureus* -infected wounds, Biomacromolecules 26 (2025) 6309–6327, https://doi.org/10.1021/acs.biomac.5c01367.
[5] Y. Yang, Y. Ren, W. Song, B. Yu, H. Liu, Rational design in functional hydrogels towards biotherapeutics, Mater. Des. 223 (2022) 111086, https://doi.org/10.1016/j.matdes.2022.111086.
[6] K.Y. Lee, D.J. Mooney, Alginate: properties and biomedical applications, Prog. Polym. Sci. 37 (2012) 106–126, https://doi.org/10.1016/j.progpolymsci.2011.06.003.
[7] K. Mukherjee, P. Dutta, A. Saha, S. Dey, V. Sahu, H. Badwaik, T.K. Giri, Alginate based semi-IPN and IPN hydrogel for drug delivery and regenerative medicine, J. Drug Delivery Sci. Technol. 92 (2024) 105402, https://doi.org/10.1016/j.jddst.2024.105402.
[8] A.O. Adebisi, P.R. Laity, B.R. Conway, Formulation and evaluation of floating mucoadhesive alginate beads for targeting Helicobacter pylori, J. Pharm. Pharmacol. 67 (2015) 511–524, https://doi.org/10.1111/jphp.12345.
[9] M. Ul-Islam, K.F. Alabbosh, S. Manan, S. Khan, F. Ahmad, M.W. Ullah, Chitosan-based nanostructured biomaterials: synthesis, properties, and biomedical applications, Adv. Ind. Eng. Polym. Res. 7 (2024) 79–99, https://doi.org/10.1016/j.aiepr.2023.07.002.
[10] N. Desai, D. Rana, S. Salave, R. Gupta, P. Patel, B. Karunakaran, A. Sharma, J. Giri, D. Benival, N. Kommineni, Chitosan: a potential biopolymer in drug delivery and biomedical applications, Pharmaceutics 15 (2023) 1313, https://doi.org/10.3390/pharmaceutics15041313.
[11] R. Biswas, S. Mondal, M.A. Ansari, T. Sarkar, I.P. Condiuc, G. Trifas, L.I. Atanase, Chitosan and its derivatives as nanocarriers for drug delivery, Molecules 30 (2025) 1297, https://doi.org/10.3390/molecules30061297.
[12] S. Eswaramma, N.S. Reddy, K.S.V.K. Rao, Carbohydrate polymer based pH-sensitive IPN microgels: synthesis, characterization and drug release characteristics, Mater. Chem. Phys. 195 (2017) 176–186, https://doi.org/10.1016/j.matchemphys.2017.04.018.
[13] N. Zoratto, P. Matricardi, Semi-IPN- and IPN-based hydrogels, Adv. Exp. Med. Biol. 1059 (2018) 155–188, https://doi.org/10.1007/978-3-319-76735-2_7.
[14] A.K. Nayak, M.S. Hasnain, T.M. Aminabhavi, Drug delivery using interpenetrating polymeric networks of natural polymers: a recent update, J. Drug Delivery Sci. Technol. 66 (2021) 102915, https://doi.org/10.1016/j.jddst.2021.102915.
[15] E.S. Dragan, D.F. Apopei, Multiresponsive macroporous semi-IPN composite hydrogels based on native or anionically modified potato starch, Carbohydr. Polym. 92 (2013) 23–32, https://doi.org/10.1016/j.carbpol.2012.08.082.
[16] G. Rassu, A. Salis, E.P. Porcu, P. Giunchedi, M. Roldo, E. Gavini, Composite chitosan/alginate hydrogel for controlled release of deferoxamine: a system to potentially treat iron dysregulation diseases, Carbohydr. Polym. 136 (2016) 1338–1347, https://doi.org/10.1016/j.carbpol.2015.10.048.
[17] T. Wu, J. Huang, Y. Jiang, Y. Hu, X. Ye, D. Liu, J. Chen, Formation of hydrogels based on chitosan/alginate for the delivery of lysozyme and their antibacterial activity, Food Chem. 240 (2018) 361–369, https://doi.org/10.1016/j.foodchem.2017.07.052.
[18] R.S. Tığlı, M. Gümüşderelioğlu, Evaluation of alginate-chitosan semi IPNs as cartilage scaffolds, J. Mater. Sci. Mater. Med. 20 (2009) 699–709, https://doi.org/10.1007/s10856-008-3624-x.

[19] N.A. Al Zahrani, R.M. El-Shishtawy, A.M. Asiri, Recent developments of gallic acid derivatives and their hybrids in medicinal chemistry: a review, Eur. J. Med. Chem. 204 (2020) 112609, https://doi.org/10.1016/j.ejmech.2020.112609.
[20] C.M.C. Andrés, J.M. Pérez de la Lastra, C.A. Juan, F.J. Plou, E. Pérez-Lebeña, Polyphenols as antioxidant/pro-oxidant compounds and donors of reducing species: relationship with human antioxidant metabolism, Processes 11 (2023) 2771, https://doi.org/10.3390/pr11092771.
[21] D.-S. Lee, J.-Y. Woo, C.-B. Ahn, J.-Y. Je, Chitosan–hydroxycinnamic acid conjugates: preparation, antioxidant and antimicrobial activity, Food Chem. 148 (2014) 97–104, https://doi.org/10.1016/j.foodchem.2013.10.019.
[22] K. Khainskaya, K. Hileuskaya, V. Nikalaichuk, A. Ladutska, O. Akhmedov, N. Abrekova, L. You, P. Shao, M. Odonchimeg, Chitosan-gallic acid conjugate with enhanced functional properties and synergistic wound healing effect, Carbohydr. Res. 553 (2025) 109496, https://doi.org/10.1016/j.carres.2025.109496.
[23] P.M. Furneri, V. Fuochi, R. Pignatello, Lipid-based nanosized delivery systems for fluoroquinolones: a review, Curr. Pharm. Des. (2017), https://doi.org/10.2174/1381612823666171122110103.
[24] M. Otto, Staphylococcal biofilms, Microbiol. Spectrum 6 (2018), https://doi.org/10.1128/microbiolspec.gpp3-0023-2018.
[25] A.E. Paharik, A.R. Horswill, The staphylococcal biofilm: adhesins, regulation, and host response, Microbiol. Spectrum 4 (2016), https://doi.org/10.1128/microbiolspec.vmbf-0022-2015.
[26] E.D. Stephens, F. Oustadi, H. Marcelo, J.L. Vierra, K. Murari, P. Egberts, M. Badv, Gradually-frozen aligned bacterial nanocellulose membranes loaded with gallic acid exhibit enhanced mechanical and dual antithrombotic-antimicrobial properties, Biomater. Sci. 13 (2025) 2673–2689, https://doi.org/10.1039/D5BM00176E.
[27] Y. Zhao, L. Yang, M. Xu, H. Wang, X. Gao, B. Niu, W. Li, Gallic acid functionalized chitosan immobilized nanosilver for modified chitosan/Poly (vinyl alcohol) composite film, Int. J. Biol. Macromol. 222 (2022) 2987–3000, https://doi.org/10.1016/j.ijbiomac.2022.10.074.
[28] C. Jeong, S. Kim, C. Lee, S. Cho, S.-B. Kim, Changes in the physical properties of calcium alginate gel beads under a wide range of gelation temperature conditions, Foods 9 (2020) 180, https://doi.org/10.3390/foods9020180.
[29] E.G. Tomarchio, C. Zagni, S. Dattilo, L. Vitiello, V. Fuochi, S. Furnari, P.M. Furneri, G. Granata, S.C. Carroccio, A. Rescifina, Advanced cyclodextrin-based multiloaded hydrogels for targeted drug delivery in the fight against vaginal fungal infections, Carbohydr. Polym. 356 (2025), https://doi.org/10.1016/j.carbpol.2025.123412.
[30] E.G. Tomarchio, V. Giglio, V. Fuochi, S. Furnari, P.M. Furneri, T. Mecca, S. Dattilo, C. Zagni, A. Rescifina, Development of a γ-cyclodextrin-based cryogel loaded with trimethoprim for acne treatment: designsynthesis, and in vitro evaluation, Int. J. Mol. Sci. 26 (2025) 6319, https://doi.org/10.3390/ijms26136319.
[31] C. Zagni, V. Patamia, S. Dattilo, V. Fuochi, S. Furnari, P.M. Furneri, S.C. Carroccio, G. Floresta, A. Rescifina, Supramolecular biomaterials as drug nanocontainers with iron depletion properties for antimicrobial applications, Mater. Adv. (2024), https://doi.org/10.1039/D3MA00918A.
[32] Y. Wang, M. Xie, G. Ma, Y. Fang, W. Yang, N. Ma, D. Fang, Q. Hu, F. Pei, The antioxidant and antimicrobial activities of different phenolic acids grafted onto chitosan, Carbohydr. Polym. 225 (2019) 115238, https://doi.org/10.1016/j.carbpol.2019.115238.
[33] M. Xie, B. Hu, Y. Wang, X. Zeng, Grafting of gallic acid onto chitosan enhances antioxidant activities and alters rheological properties of the copolymer, J. Agric. Food Chem. 62 (2014) 9128–9136, https://doi.org/10.1021/jf503207s.
[34] J. Liu, H. Yong, Y. Liu, R. Bai, Recent advances in the preparation, structural characteristics, biological properties and applications of gallic acid grafted polysaccharides, Int. J. Biol. Macromol. 156 (2020) 1539–1555, https://doi.org/10.1016/j.ijbiomac.2019.11.202.
[35] X. Hu, Y. Wang, L. Zhang, M. Xu, Morphological and mechanical properties of tannic acid/PAAm semi-IPN hydrogels for cell adhesion, Polym. Test. 61 (2017) 314–323, https://doi.org/10.1016/j.polymertesting.2017.05.034.
[36] J. Liu, J. Lu, J. Kan, C. Jin, Synthesis of chitosan-gallic acid conjugate: Structure characterization and *in vitro* anti-diabetic potential, Int. J. Biol. Macromol. 62 (2013) 321–329, https://doi.org/10.1016/j.ijbiomac.2013.09.032.
[37] C. Peniche-Covas, W. Argüelles-Monal, J. San Román, A kinetic study of the thermal degradation of chitosan and a mercaptan derivative of chitosan, Polym. Degrad. Stab. 39 (1993) 21–28, https://doi.org/10.1016/0141-3910(93)90120-8.
[38] L. Quiles-Carrillo, S. Montava-Jordà, T. Boronat, C. Sammon, R. Balart, S. Torres-Giner, On the use of gallic acid as a potential natural antioxidant and ultraviolet light stabilizer in cast-extruded bio-based high-density polyethylene films, Polymers (Basel) 12 (2019) 31, https://doi.org/10.3390/polym12010031.
[39] S. Kumar, B. Singh, Designing zwitterionic-polysaccharide network hydrogels by covalent and non-covalent functionalization for drug delivery applications, Int. J. Biol. Macromol. (2025) 148468, https://doi.org/10.1016/j.ijbiomac.2025.148468.
[40] M. Rinaudo, Chitin and chitosan: properties and applications, Prog. Polym. Sci. 31 (2006) 603–632, https://doi.org/10.1016/j.progpolymsci.2006.06.001.
[41] K. Baysal, A.Z. Aroguz, Z. Adiguzel, B.M. Baysal, Chitosan/alginate crosslinked hydrogels: preparation, characterization and application for cell growth purposes, Int. J. Biol. Macromol. 59 (2013) 342–348, https://doi.org/10.1016/j.ijbiomac.2013.04.073.
[42] C. Zagni, A. Coco, T. Mecca, G. Curcuruto, V. Patamia, K. Mangano, A. Rescifina, S. C. Carroccio, Sponge-like macroporous cyclodextrin-based cryogels for controlled drug delivery, Mater. Chem. Front. 7 (2023) 2693–2705, https://doi.org/10.1039/D3QM00139C.
[43] T.S. Pathak, J.-H. Yun, J. Lee, K.-J. Paeng, Effect of calcium ion (cross-linker) concentration on porosity, surface morphology and thermal behavior of calcium alginates prepared from algae (*Undaria pinnatifida*), Carbohydr. Polym. 81 (2010) 633–639, https://doi.org/10.1016/j.carbpol.2010.03.025.
[44] L. Nicolle, C.M.A. Journot, S. Gerber-Lemaire, Chitosan functionalization: covalent and non-covalent interactions and their characterization, Polymers (Basel) 13 (2021) 4118, https://doi.org/10.3390/polym13234118.
[45] G.R. Park, M.A. Gwak, Y.H. Choi, W.H. Park, pH-sensitive gallol-rich chitosan hydrogel beads for on-off controlled drug delivery, Int. J. Biol. Macromol. 240 (2023) 124346, https://doi.org/10.1016/j.ijbiomac.2023.124346.
[46] L. Li, L. Ren, Q. Zhao, K. Xu, Q. Wu, Q. Su, X. Li, X. Lü, L. Wang, Gallic acid-grafted chitosan photothermal hydrogels functionalized with mineralized copper-sericin nanoparticles for MRSA-infected wound management, Carbohydr. Polym. 352 (2025) 123179, https://doi.org/10.1016/j.carbpol.2024.123179.
[47] G. He, X. Yan, Z. Miao, H. Qian, Y. Ma, Y. Xu, L. Gao, Y. Lu, Z. Zha, Anti-inflammatory catecholic chitosan hydrogel for rapid surgical trauma healing and subsequent prevention of tumor recurrence, Chin. Chem. Lett. 31 (2020) 1807–1811, https://doi.org/10.1016/j.cclet.2020.02.032.
[48] W. Weian, Y. Yunxin, W. Ziyan, J. Qianzhou, G. Lvhua, Gallic acid: design of a pyrogallol-containing hydrogel and its biomedical applications, Biomater. Sci. 12 (2024) 1405–1424, https://doi.org/10.1039/D3BM01925J.
[49] I. Best, S. Casimiro-Gonzales, A. Portugal, L. Olivera-Montenegro, L. Aguilar, A. M. Muñoz, F. Ramos-Escudero, Phytochemical screening and DPPH radical scavenging activity of three morphotypes of *Mauritia flexuosa* L.f. from Peru, and thermal stability of a milk-based beverage enriched with carotenoids from these fruits, Heliyon 6 (2020) e05209, https://doi.org/10.1016/j.heliyon.2020.e05209.
[50] M. Hadidi, R. Liñán-Atero, M. Tarahi, M.C. Christodoulou, F. Aghababaei, The potential health benefits of gallic acid: therapeutic and food applications, Antioxidants (Basel) 13 (2024) 1001, https://doi.org/10.3390/antiox13081001.
[51] L. Wang, C. Hu, L. Shao, The antimicrobial activity of nanoparticles: present situation and prospects for the future, IJN 12 (2017) 1227–1249, https://doi.org/10.2147/IJN.S121956.